Distinct dynamics and interaction patterns in H- and K-Ras oncogenic P-loop mutants

Abdallah Sayyed-Ahmad [ORCID], Priyanka Prakash, and Alemayehu A. Gorfe*

Department of Integrative Biology and Pharmacology, University of Texas Health Science Center at Houston, Houston, Texas, 77030

ABSTRACT

Despite years of study, the structural or dynamical basis for the differential reactivity and oncogenicity of Ras isoforms and mutants remains unclear. In this study, we investigated the effects of amino acid variations on the structure and dynamics of wild type and oncogenic mutants G12D, G12V, and G13D of H- and K-Ras proteins. Based on data from μs-scale molecular dynamics simulations, we show that the overall structure of the proteins remains similar but there are important differences in dynamics and interaction networks. We identified differences in residue interaction patterns around the canonical switch and distal loop regions, and persistent sodium ion binding near the GTP particularly in the G13D mutants. Our results also suggest that different Ras variants have distinct local structural features and interactions with the GTP, variations that have the potential to affect GTP release and hydrolysis. Furthermore, we found that H-Ras proteins and particularly the G12V and G13D variants are significantly more flexible than their K-Ras counterparts. Finally, while most of the simulated proteins sampled the effector-interacting state 2 conformational state, G12V and G13D H-Ras adopted an open switch state 1 conformation that is defective in effector interaction. These differences have implications for Ras GTPase activity, effector or exchange factor binding, dimerization and membrane interaction.

INTRODUCTION

The Ras family small GTPases propagate signal from cell-surface receptors to crucial signal transduction cascades including the mitogen-activated protein kinase/extracellular signal-regulated kinase (MAPK/ERK) and phosphatidylinositol-4,5-bisphosphate 3-kinas/Protein kinase B (PI3K/AKT) pathways.[1] They are on/off switches that regulate cell proliferation, growth, and development by interconverting between GTP- and GDP-bound forms.[2] Active and inactive Ras primarily differ at two flexible switch regions: switch SI (residues 25–40) and SII (residues 60–75).[3–6] The switch regions undergo nucleotide-dependent conformational changes that allow them to selectively interact with exchange factors or effectors.[7,8] Recent studies suggest that the bound nucleotide may also modulate Ras dimerization,[9] clustering,[10] and membrane binding.[11–14]

Despite a nearly identical catalytic domain (residues 1–166, see Fig. 1), the three most common Ras isoforms in human cells (N-, H-, and K-Ras) respond to extracellular stimuli in a divergent although controlled fashion.[15–17] As a result, their malfunction can lead to distinct cancer types. These include H-Ras mutations in

thyroid[18] and bladder cancers,[19] K-Ras mutations in lung, colorectal,[20] and pancreatic cancers,[21] and N-Ras mutations in melanomas and hematologic malignancies.[22,23] In general, mutant Ras is associated with about a quarter of all human cancers and K-Ras mutations account for 85% of the Ras-related cancers.[23–25] Consequently, K-Ras has become one of the most prominent anticancer drug targets.[26–32] The isoforms significantly differ in sequence at the hypervariable region (HVR, residues 167–185/6) that anchors Ras to the inner leaflet of the plasma membrane. Membrane binding is achieved through a post-translationally farnesylated C-terminus
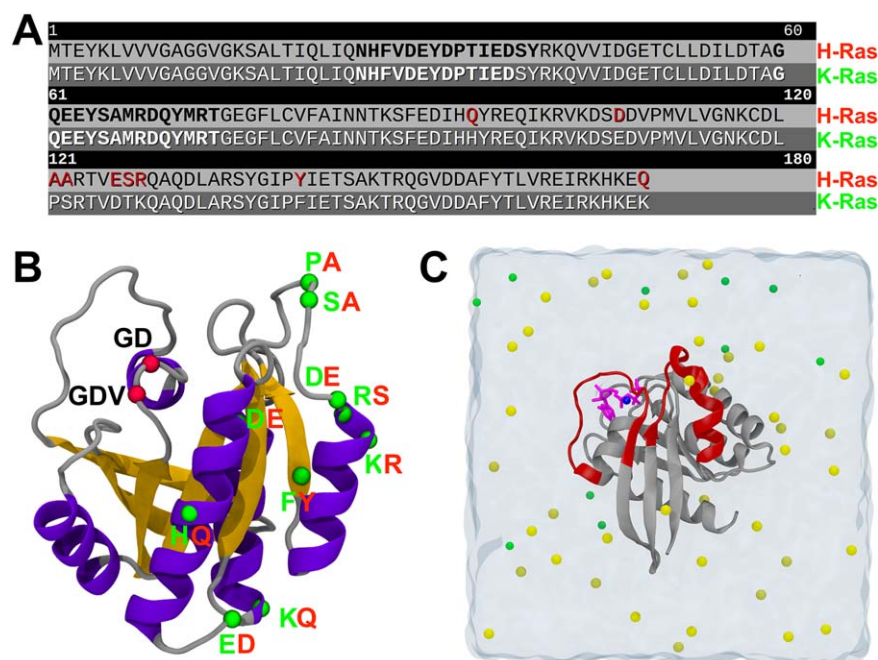
Figure 1

H- and K-Ras sequence and structure. (**A**) Sequence alignment of the catalytic domain of WT H- and K-Ras proteins. The SI and SII regions are highlighted by bold font, while the sequence differences between the two proteins are highlighted in red. (**B**) K-Ras structure shown in cartoon with the location of the mutations studied in this work highlighted by red spheres. Similarly, isoform variations are highlighted by green spheres and labeled in green and red for K-Ras and H-Ras, respectively. (**C**) A snapshot from one of the simulations; the catalytic domain is in cartoon colored in dark grey with switches SI (residues 25–40) and SII (residues 60–75) in red. Water is shown as transparent light cyan shading with magnesium, sodium and chloride ions in blue, yellow and green spheres, respectively. The bound GTP is in purple sticks. [Color figure can be viewed at wileyonlinelibrary.com]

complemented by a proximal palmitoylated cysteine (N- and H-Ras) or polybasic domain (K-Ras).[33] Thus the HVR regulates isoform-specific plasma membrane distribution,[11,13,34] but the role of the few amino acid substitutions at the catalytic domain is not clear.

Differential engagement with membrane, regulators, or effectors defines the complexity of Ras signaling.[35,36] Functional differences among Ras isoforms or mutants, however, are likely determined by an intricate interplay of minimally altered interactions. This makes the interpretation of cell-based experimental data (e.g., see Ref. 37) in terms of an underlying molecular mechanism a very challenging task. Several studies have suggested that Ras functional diversity might involve variations in the population of conformational states spanning a spectrum of inactive, intermediate, and active states.[38–40] In addition to the bound nucleotide[38,41] and mutations[40,42–44] (see also more recent elegant calculations on the impact of mutations on GTP hydrolysis[45–47]) the population of these states may be affected by oligomerization and interaction with membrane or other partners.[11–13,48–52] Interaction with partner proteins can induce relatively large conformational changes especially at the switch loops.[53–55] However, mutations, including oncogenic somatic point mutations,[24,31] induce only small changes that are difficult to unambiguously link to functional consequences. In

particular, mutations at positions 12 and 13 of the phosphate-binding P-loop cause only subtle local conformational changes in the average structure and yet lead to distinct cancer phenotypes.[22] A number of studies have suggested that oncogenic mutations vary in their effects on effector or regulator binding,[56–59] but little measurable changes in structure, dynamics, or inter-residue interaction profile have been documented. Moreover, the vast majority of the available X-ray and NMR structures do not contain GTP but rather GDP or a nonhydrolyzable GTP analog. Thus it remains unclear how mutations affect the dynamics of GTP-Ras. Based on a detailed analysis of unbiased molecular dynamics (MD) simulations, here we show that wild type (WT) H- and K-Ras and their oncogenic G12D, G12V, and G13D variants exhibit differential structural adaptions and fluctuations in the ns–μs timescale.

MATERIALS AND METHODS

We simulated the GTP-bound catalytic domain of WT H- and K-Ras, and three mutants of each: G12D, G12V, and G13D. As shown in Figure 1, all the mutations considered here are on the P-loop at lobe 1 (residues 1–86) whereas the isoform variations are located at lobe 2 (residues 87–166).[60]

Initial structures and system setup

For G12D K-Ras, the starting structure was downloaded from the RCSB protein data bank (pdb id: 4DSO). Since high-resolution crystal structure was unavailable for WT and G12V K-Ras, we used this same 4DSO structure to generate their initial configurations by mutating D12 to G or V. Similarly, we mutated D12 to G and G13 to D in the 4DSO structure to generate a G13D mutant K-Ras structure. For WT H-Ras and its G12V and G12D variants, we used the available crystal structures 1QRA, 2VH5, and 1AGP, respectively. We mutated G13 to D in the 1QRA structure to generate the starting structure of G13D H-Ras. In each case we replaced the GTP analog to GTP and removed all other atoms/molecules in the PDB file except for waters and Mg^{2+}. The C-terminus and anionic residues were deprotonated while the N-terminus and cationic residues were protonated assuming neutral pH. The resulting structure was placed in a cubic box containing TIP3P water molecules, and Na^+ and Cl^- ions were added to neutralize the system and achieve an ionic strength of 150 mM (Supporting Information Table S1). A minimum of 10 Å buffer between the edges of the box and protein atoms was used to ensure that the protein does not interact with its periodic images. Figure 1(C) shows an example of the final system configuration.

Molecular dynamics simulation

The solvated systems were energy minimized (5000 steps of conjugate gradient), gradually heated keeping the Cα and GTP heavy atoms restrained by a harmonic restraint of force constant $k = 4$ kcal mol^{-1} Å^{-2} and equilibrated with k progressively reduced to zero by decrements of 1 kcal mol^{-1} Å^{-2} every 100 ps. A 2 fs time step was used with the SHAKE[61] algorithm applied to covalent bonds involving hydrogen atoms. The isothermal–isobaric (NPT) ensemble and periodic boundary conditions were used. Temperature was maintained at the physiologic value of 310 K using Langevin dynamics with a damping coefficient of 10 ps^{-1}. The Nose-Hoover Langevin piston method was used with a piston period of 200 fs and decay time interval of 100 fs to maintain constant pressure at 1.0 atm. Short-range van der Waals interactions were smoothly switched off between 10 Å and 12 Å, with a 14 Å cutoff used for nonbonded pair list updates. Long-range electrostatic interactions were computed using the Particle Mesh Ewald (PME) method[62] with grid density of about one grid point per Å. Each system was simulated for 1 μs with NAMD2.11[63] using the CHARMM27 empirical force field and CMAP dihedral angle correction.[64]

Residue contact analysis

Coarse-grained residue–residue contact analysis has been successfully used to examine dynamic interactions in proteins.[60,65,66] While sufficient for most applications, residue–residue contact would miss cases in which, for example, a side-chain reorientation occurs while backbone contact remains intact. To capture subtle conformational changes that might be missed by the traditional approach, we developed a version that splits the residue–residue contact into backbone– and side-chain–residue contacts. Thus, we defined contact based on a distance cutoff of 4.5 Å between two heavy atoms of the (i) backbone of residue i and backbone or side-chain of residue j (backbone–residue contact) and (ii) side-chain of the ith residue and backbone or side-chain of the jth residue (side-chain–residue contact). Backbone (b_{ij}) and side-chain (s_{ij}) binary contact state variables were then assigned a value of 1 if contact exists and 0 otherwise. The corresponding contact probabilities $\langle b_{ij} \rangle$ and $\langle s_{ij} \rangle$ were calculated by averaging s_{ij} and b_{ij} over the entire trajectory and then symmetrized on the maximum. Similarly, we split GTP into three contact moieties: purine, ribose, and triphosphate. To quantify conformational differences between two trajectories, a single difference contact measure (dc_{ij}) was constructed using a signed Chebyshev distance to merge the difference backbone– and side-chain–residue contact probabilities:

$$dc_{ij} = \begin{cases} \langle s_{ij} \rangle_{\mathrm{m}} - \langle s_{ij} \rangle_{\mathrm{ref}} & if \ |\langle s_{ij} \rangle_{\mathrm{m}} - \langle s_{ij} \rangle_{\mathrm{ref}}| > |\langle b_{ij} \rangle_{\mathrm{m}} - \langle b_{ij} \rangle_{\mathrm{ref}}| \\ \langle b_{ij} \rangle_{\mathrm{m}} - \langle b_{ij} \rangle_{\mathrm{ref}} & \text{otherwise} \end{cases}$$

(1)

where subscript m and ref denote two different trajectories. To ensure statistical significance of the observed dc_{ij} only residue pairs with interaction probability differences of ≥40% were considered.

Calculation of backbone relaxation times and NMR order parameter

Changes in entropy and allostery associated with conformational dynamics generally affect interactions of a protein with its binding partners. Likewise, differences among Ras proteins in terms of amplitude and frequency of residue fluctuations could impact intermolecular interactions. Previous studies[67–71] suggested that backbone motions in Ras are mostly of small amplitude and occur on a long timescale. However, the switch regions have been shown to undergo high frequency large amplitude fluctuations.[41,68,69] Therefore, we first examined the dynamics of SI and SII based on the relaxation of their backbone N—H dipoles using the correlation function $C(t)$[72] defined as

$$C(t) = \langle P_2(\hat{\mu}_t \cdot \hat{\mu}_0) \rangle \qquad (2)$$

where P_2 is the second-order Legendre polynomial and $\hat{\mu}$ is a unit vector along the backbone amide N—H bond at times t and 0. The angle brackets denote averaging over
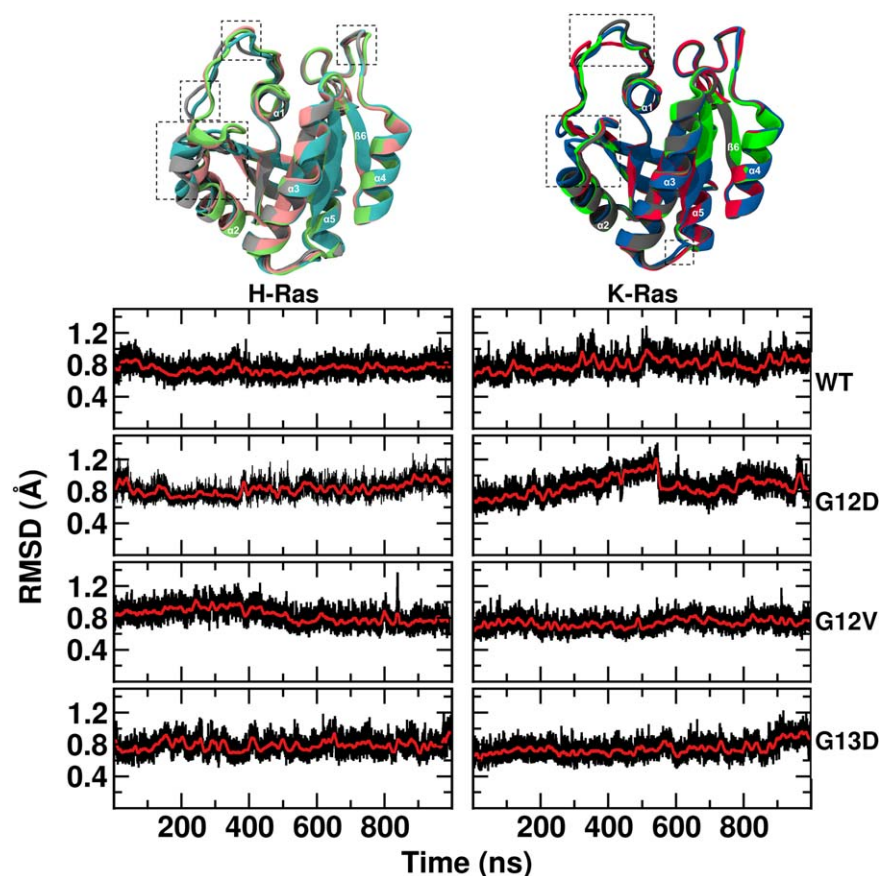
Figure 2

Time evolution of backbone RMSD. (Top) Time-averaged backbone structure of H-Ras and K-Ras mutants. Dashed squares highlight regions with significant conformational differences. (Bottom) Time evolution of backbone RMSD from the respective initial X-ray structure calculated after alignment excluding the flexible switch regions. Sampling was every 10 ps (black) with 10 ns-running averages (red). Color codes in this and subsequent figures are as follows. K-Ras: G12D (black), G13D (dark red), G12V (dark blue), and WT (dark green); H-Ras: G12D (grey), and G13D (light red), G12V (light blue), and WT (light green). [Color figure can be viewed at wileyonlinelibrary.com]

time, time origins, and N—H bonds of SI or SII. The internal backbone correlation function, $C_{int}(t)$, was calculated similarly after removing the center of mass translational and rotational motions by aligning each frame to the initial structure excluding the switches.

To probe the dynamics in the entire protein including long timescale and small amplitude fluctuations, we calculated the NMR order parameter per residue, S^2, using[73]

$$S^2 = \frac{3}{2}\left[\langle\mu_x^2\rangle^2 + \langle\mu_y^2\rangle^2 + \langle\mu_z^2\rangle^2 + 2\langle\mu_x\mu_y\rangle^2 + 2\langle\mu_x\mu_z\rangle^2 + 2\langle\mu_y\mu_z\rangle^2\right] - \frac{1}{2}$$

(3)

where μ_x, μ_y, and μ_z are the x, y, and z components of $\hat{\mu}$ of a given residue. S^2 is averaged over the entire trajectory and has contributions from all internal motions irrespective of timescales.

RESULTS AND DISCUSSION

We used eight 1-μs-long unbiased MD simulations of H- and K-Ras catalytic domains to map out the structural and dynamic features behind the functional divergence of Ras isoforms and mutants. Below we describe the differential dynamics of these systems as assessed by principal component (PC) analysis, a combined backbone–residue and side-chain–residue contact analysis, relaxation order parameters, and other detailed trajectory analysis techniques.

H-Ras mutants exhibit larger global dynamics than K-Ras

Overlay of the average structure from each of the eight simulations (Fig. 2, top) indicate no major structural differences at the core of the different Ras proteins studied in this work. The overall structure is very stable in all of the simulations, with <1.2 Å backbone root square mean deviation (RMSD) from the respective X-ray structures
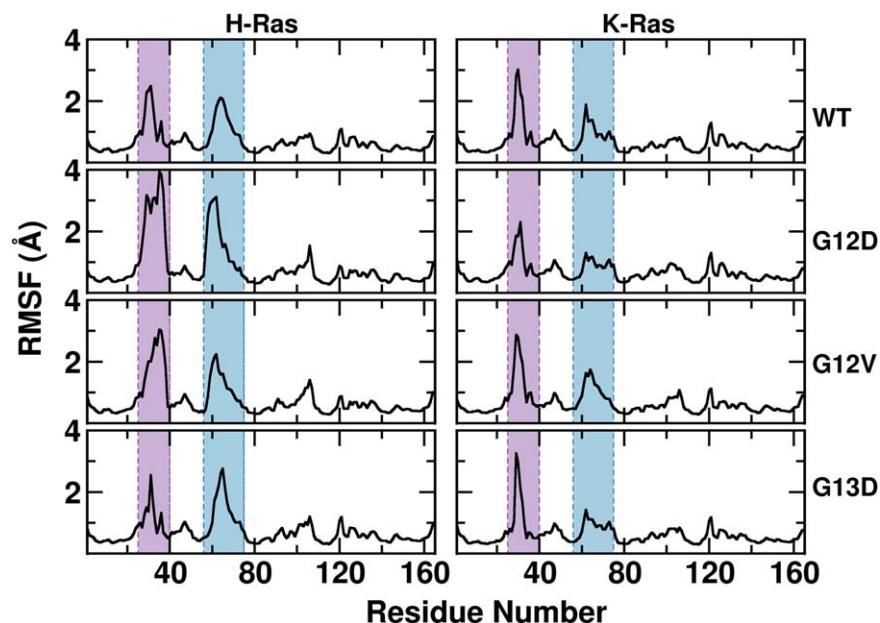
Figure 3

Cα RMSF. Backbone RMSF calculated after alignment excluding SI and SII that are highlighted by purple and cyan shadow, respectively. [Color figure can be viewed at wileyonlinelibrary.com]

(Fig. 2, bottom). However, notable differences are apparent at SI and SII (Supporting Information Figure S1–2). For SI, the average RMSD of the mutants relative to WT is 0.75–1.6 Å (K-Ras) and 0.71–4.0 Å (H-Ras); G12D and G12V H-Ras have the largest RMSD and adopted an open SI conformation. Similarly, the RMSDs of SII are large: 1.3–2.4 Å for K-Ras and 0.6–3.2 Å for H-Ras; this is mainly due to conformational changes at the N-terminus of α2. These are mirrored by the Cα atom root-mean square fluctuations (RMSFs) per residue, which are indistinguishable among most of the proteins except at a few residues of SI and SII (Fig. 3). In particular, SI is most flexible in G12D and G12V H-Ras, while it is least flexible in G13D and WT H-Ras and G12D K-Ras. All K-Ras mutants exhibit markedly less flexibility at SII. Overall, these results suggest that H-Ras proteins are more flexible than K-Ras at least for the variants studied here. This is in contrast with our earlier findings based on short (10–20 ns) simulations of G12V and A59G H-Ras on the one hand and homology-built G12V K-Ras and Q61H K-Ras on the other, where the K-Ras variants were found to be more flexible at SI, SII, and other loop regions.[43,60]

To further examine the global dynamics of the simulated systems we used a previously described approach.[41,60] This approach entails a PC analysis of Ras X-ray structures and projection of MD-derived conformations onto an *xy*-plane defined by the two PCs with the largest eigenvalues. Figure 4 shows that our proteins sample a relatively wide but largely overlapping

conformational space close to the cluster of GTP-Ras X-ray structures. Despite the overall similarities, however, two important lessons could be drawn from this analysis regarding the dynamic signature of the simulated systems. First, the H-Ras systems sampled a larger conformational space than their K-Ras counterparts. This is substantiated by the observed fluctuations along PC1 due to large fluctuations of SI (Supporting Information Table S2). Secondly, G12D and G12V H-Ras sample regions in-between those sampled by GDP- and GTP-bound X-ray structures. This suggests that these mutants adopt an intermediate conformation, in agreement with our previous observation for G12V H-Ras.[60]

Backbone– and side-chain–residue contact analysis reveals differential interaction networks in H- and K-Ras isoforms and their P-loop oncogenic mutants

We first analyzed our trajectories using the more coarse residue–residue contact analysis described in previous reports.[60,65,66] We noticed that this analysis failed to capture a few differential dynamic contacts that were apparent during visual inspection. For example, side chains of E31 and D33, residues critical for effector binding,[74] form a metal ion-mediated salt bridge 60% of the time in WT H-Ras but almost never in G12D H-Ras. Since E31 and D33 are sequence neighbors, their backbone atoms remain close and yield a high residue–residue contact probability in both WT and G12D H-Ras. For these residues, the difference in
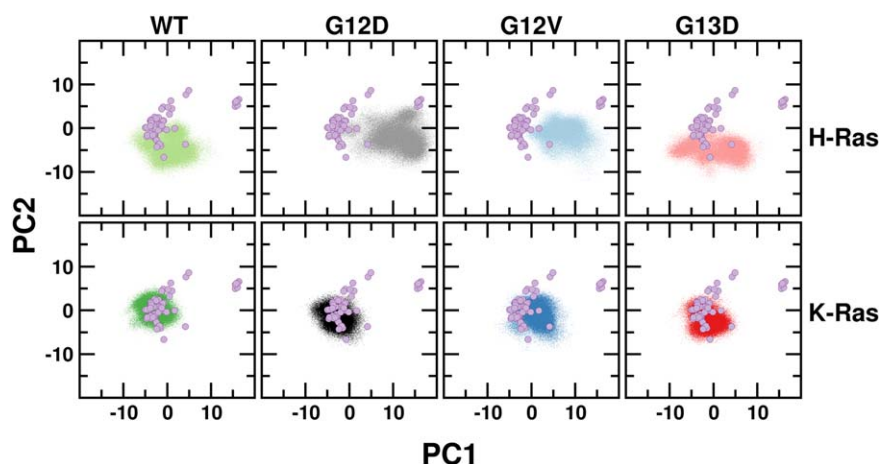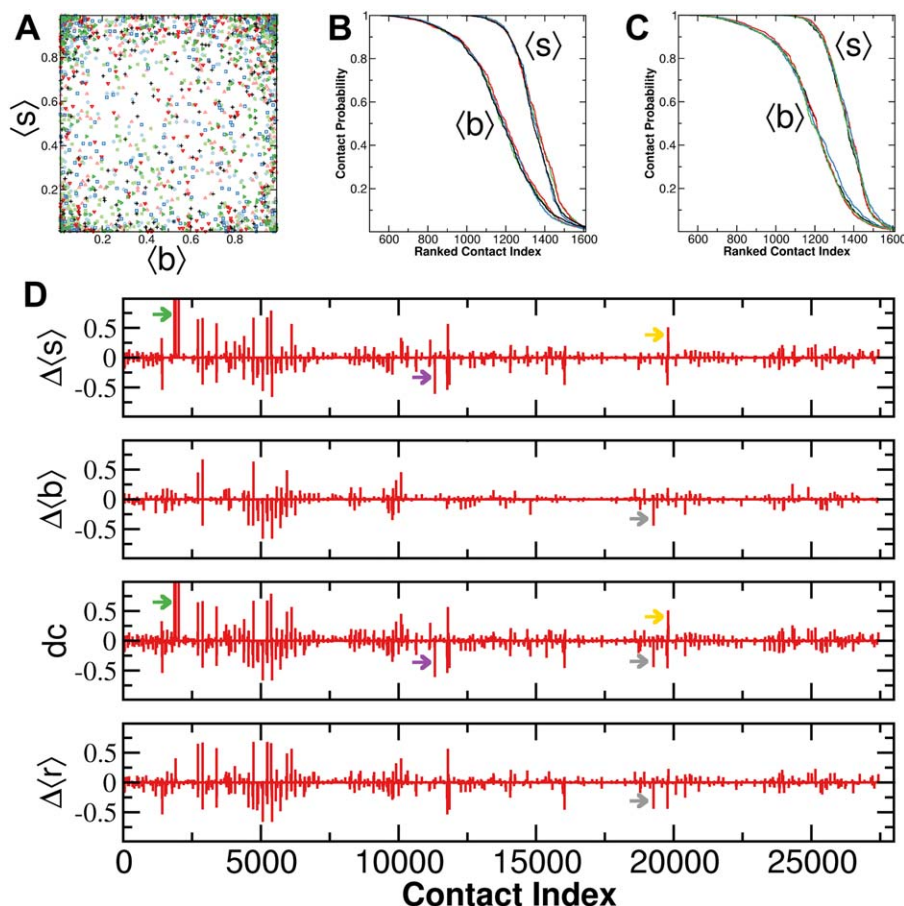
Figure 4

Global conformational dynamics of H- and K-Ras mutants. Projection of simulated conformations onto the first and second principal components obtained from an analysis of Ras crystallographic structures (purple circles). [Color figure can be viewed at wileyonlinelibrary.com]

contact probability between the trajectories would therefore be zero. We reasoned that a slightly more fine-grained contact analysis that entails combined side-chain–residue and backbone–residue contacts would capture the metal-mediated interaction between E31 and D33, as well as similar other dynamic interactions. Figure 5(A) shows the wide spectrum of backbone– and side-chain–residue contact probability patterns for H- and K-Ras mutants. As expected, residue–residue interactions occur through a combination of backbone–residue (along x axis), side-chain–residue (along y axis), or both (the rest of the x–y plane). Figure 5(B,C) show the rank ordered probabilities of backbone–residue and side-chain–residue contacts. Despite the small variations in the number of interactions and their persistence among the mutants and isoforms, no major inter-residue contact perturbations were observed. This is consistent with the absence of global conformational changes, as described in the previous section. The difference between the side-chain– and backbone–residue rank ordered contact probabilities indicates that side chains have larger contribution to the inter-residue interaction network. The sharp transition in the side-chain-residue ranked contact probability curves indicates fewer number of transient side-chain–residue interactions than backbone–residue interactions.

In order to compare two Ras variants, we merged the side-chain– and backbone–residue contact probabilities into one measure using a signed Chebyshev distance (Eq. (1)). Using WT and G12D K-Ras as an example, Figure 5(D) shows how this measure preserves the largest differences in side-chain– and backbone–residue contact probabilities. However, there are some notable differences between the fine-grained and coarse-grained analyses. These include interactions of D/G12 with neighboring

residues (green arrow) that are captured by the difference in side-chain–residue ($\Delta\langle s\rangle$) but not by residue–residue ($\Delta\langle r\rangle$) or backbone–residue ($\Delta\langle b\rangle$) contact probabilities. Similarly, the yellow and purple arrows highlight differences captured only by $\Delta\langle s\rangle$, including R68-Y71 and C118-S145 interactions. These observations demonstrate the additional insights that can be obtained from splitting the contact analysis into its side-chain and backbone components.

Using this approach, Figure 6 shows differences in interaction patterns among all of the simulated systems. One can see that there are a large number of variations within and in the vicinity of the nucleotide-binding site, plus a few at relatively distant locations. A number of important observations can be made from Figure 6. (i) The hydroxyl group of Y32 is engaged in a hydrogen bond interaction with the backbone amide of V29 in G12V K-Ras whereas in G12D and G13D H-Ras it frequently interacts with the α-phosphate oxygen atoms. In the rest of the mutants and WT H- and K-Ras, Y32 is flexible with no significant preferred interactions. These variations may have functional significance since Y32 undergoes a major reorientation during nucleotide exchange.[68,75,76] (ii) We observe variations in the persistence of the network of interactions involving Y71 and V9, E37, D38, or R68. Many of these residues are part of a proposed dimerization interface,[77] and a ligand binding pocket[30,78–80] whose solvent accessibility may be affected by these variations. For instance, displacement of Y71 exposes the hydrophobic cleft around residues V7, V9, F58, and F78. (iii) Most mutants show increased coupling between SII and SI relative to the WT proteins. This was made possible by the formation of transient contacts between the SII residue Y71 and the effector interacting SI residues E37 and D38. In particular, the side-chain of Y71
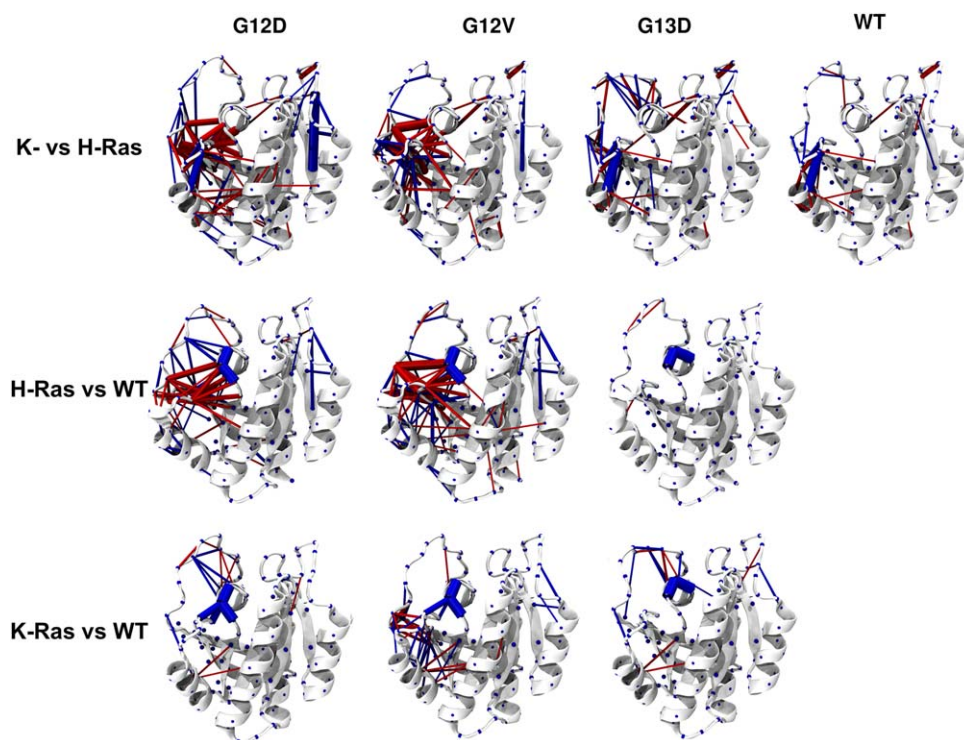
Figure 5

Combined backbone–residue and side-chain–residue contact analysis. (**A**) Scatter plot of side-chain–residue versus backbone–residue contacts of all possible residue pairs from all simulated systems. (**B, C**) Backbone–residue ($\langle b \rangle$) and side-chain–residue ($\langle s \rangle$) probability of contacts ranked by occurrence for H-Ras proteins (**B**) and K-Ras proteins (**C**). (**D**) Difference in side-chain–residue ($\Delta\langle s \rangle$), backbone–residue ($\Delta\langle b \rangle$), and residue–residue ($\Delta\langle r \rangle$) contact probabilities between G12D and WT K-Ras. $\Delta\langle s \rangle$ and $\Delta\langle b \rangle$ were merged into a single difference measure (dc) using a signed Chebyshev distance (Eq. (1)). Green, purple, and yellow arrows highlight a more significant change in side-chain–residue contact probability, while grey arrows highlight a change in backbone–residue contact probability that is also captured by the difference in residue–residue contact probabilities. [Color figure can be viewed at wileyonlinelibrary.com]

frequently interacts with the side-chain or backbone atoms of E37 or D38 in all of the mutants except G12V H-Ras, where Y71 interacts with the proximal A59. Also, Y71 sporadically couples SII and α3 through its interaction with Y96. (iv) Y96 and R68 are engaged in a stable interaction in the K-Ras proteins, but less so in G12V and WT H-Ras and it is entirely lost in G12D and G13D H-Ras. These observations strongly suggest that P-loop mutations have the potential to affect Ras self-interaction[81] and membrane orientation,[13,49] processes that have been shown to involve α3 and SII. (v) In H-Ras proteins, α2 is elongated and Y141 and R123 form a hydrogen bond. The latter is absent in K-Ras due to the Y141F substitution. Overall, these variations in intraprotein interaction networks around the active site will likely affect GTP hydrolysis and/or GDP release or may differentially induce indirect allosteric effects.

Dynamics of protein–GTP interactions

Given the variable intraprotein interaction patterns described above, we wondered whether mutations at positions 12 and 13 might also affect protein–GTP interactions. This is important because these interactions can affect rates of nucleotide exchange and GTPase activity. Therefore, we first looked at the distribution of the total number of protein–GTP contacts. We found that the average number and fluctuation of these contacts are generally insensitive to mutation; the exception is G12D H-Ras that have a smaller average number of contacts. In the G13D mutants the aspartate forms an ion-mediated interaction with Oγ1 of GTP, which may affect the kinetics of nucleotide binding and release. This is consistent with biochemical experiments that found that the intrinsic rate of GDP/GTP exchange in G13D K-Ras is an order of magnitude higher than WT.[57] These

Figure 6
Difference contact probability networks. Residue pairs of a protein that show |dc| of 40% or more relative to another mutant or isoform are connected by cylinders whose radius is weighted by |dc| and colored in blue (gain of interaction) or red (loss of interaction). (Top) Difference contact probabilities of K-Ras proteins from their H-Ras counterparts. (Middle) Difference contact probabilities of H-Ras mutants relative to WT H-Ras. (Bottom) Difference contact probabilities of K-Ras mutants relative to WT K-Ras. Notice that in both K-Ras and H-Ras, G13D exhibits the least difference from the WT, possibly because even a 1 μs run may not be sufficient to completely relax the system in response to the mutagenesis.

results show that individual P-loop mutations variably affect interactions with the bound GTP in a manner that impacts function.

Earlier ^{31}P NMR experiments on H-Ras bound to guanosine 5′-(β, γ-imido) triphosphate (GppNHp, a nonhydrolyzable GTP analog) found two slowly exchanging conformational states (state 1 and 2), with distinct chemical shift values for the phosphate atoms of the nucleotide.[38,82,83] Conformational state 2 interacts with effector proteins while state 1 favors exchange factors[38,82] and/or acts as a reservoir of the GTP·Ras pool.[84] Our simulated structures mostly remained close to the initial state 2 configuration. For instance, interactions of T35 and G60 with GTP that are characteristic of state 2 are very similar in all mutants except G12D and G12V H-Ras as assessed by inter-atomic distances (Table I). In G12D and G12V H-Ras, the average G60:N-GTP:$O_{\gamma 2}$ and T35:Oη-GTP:Oγ3 distances are significantly larger, because the interactions were lost very early in the simulations and did not recover. This suggests that GTP-bound G12D and G12V H-Ras predominantly sample the inactive state 1 conformation, similar to the X-ray structure 2Q21 of G12V H-Ras where the

switch regions are very flexible and less coupled,[85] and the state 1 T35S H-Ras structure bound to GppNpH.[86] However, despite the flexibility of the switches, G12V H-Ras forms unique and persistent interactions with the GTP ribose O1′ and O2′ via A29 and D30. These interactions appear to have attenuated the fluctuation of the switch regions when compared to G12D H-Ras. Overall, our results support the notion that SI of GTP-Ras exists in multiple conformational states including states 1 and 2. The fact that we did not observe multiple transition events between these states suggests that interstate

Table I
Average Distance of T35 and G60 from GTP

|	G60:N-GTP:$O_{\gamma 2}$ (Å)	T35:O_η-GTP:$O_{\gamma 3}$ (Å)
WT H-Ras	3.6 ± 0.5	2.9 ± 0.1
G12D H-Ras	7.4 ± 1.2	10 ± 2
G12V H-Ras	6.4 ± 0.5	11 ± 2
G13D H-Ras	3.3 ± 0.4	2.9 ± 0.1
WT K-Ras	3.5 ± 0.5	2.8 ± 0.1
G12D K-Ras	3.1 ± 0.3	2.9 ± 0.1
G12V K-Ras	3.4 ± 0.6	2.9 ± 0.4
G13D K-Ras	3.2 ± 0.3	2.9 ± 0.1
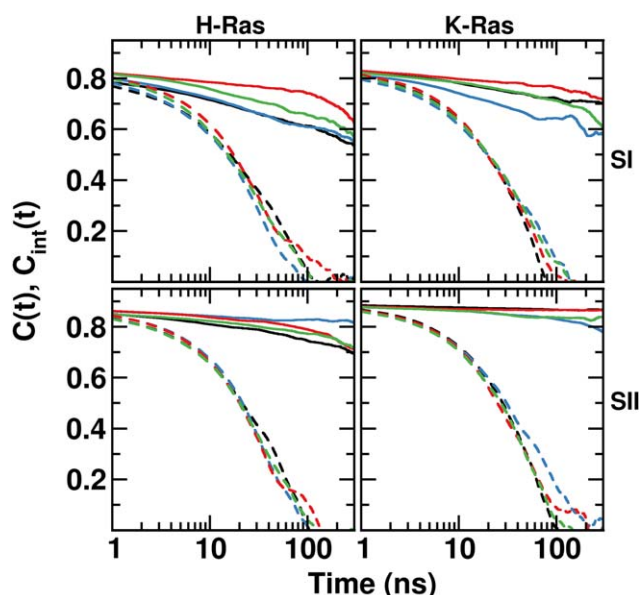
Figure 7

Internal and total dynamics correlation functions. Shown are backbone amide bond dipole relaxations of the switch regions with total ($C(t)$) and internal ($C_{int}(t)$) correlation functions shown as dashed and solid lines, respectively. Color code as in Figure 2. [Color figure can be viewed at wileyonlinelibrary.com]

transitions, particularly the transition from state 1 to state 2, are slow processes that occur on timescales >1 μs.

H- and K-Ras mutants exhibit differential relaxation times and backbone order

To probe effects of mutations on the relaxation times and internal motions of the switch regions, we computed the total ($C(t)$) and internal ($C_{int}(t)$) correlation functions of the backbone amides. Figure 7 shows that for both SI and SII, $C(t)$ and $C_{int}(t)$ are characterized by an initial steep decline followed by a slow decay. The initial decay can be linked to amide bond vibrations followed by fast local fluctuations while the slower phase can be linked to internal conformational flexibility. The $C(t)$ plots, which describe the overall rotational motion of the switch regions, decay very slowly over an extended time, and diverge from the $C_{int}(t)$ within a few nanoseconds due to molecular tumbling. Overall, $C_{int}(t)$ suggests that in the 1–50 ns time range SI has faster relaxation dynamics and is more flexible than SII. It also shows that the G13D mutation induces the slowest (and the least) and G12V the fastest (and the largest) SI relaxation within the same timescale. G12D and G13D K-Ras and G12V H-Ras exhibit a slower SII relaxation than the rest of the mutants, suggesting that the other mutants are likely to experience faster timescale transitions. These observations are supported by the calculated amide backbone order parameter per residue, S^2 (Fig. 8 and Supporting Information Fig. S3) (S^2 was calculated over the entire trajectory at sampling frequency of 0.2 ns, but other sampling frequencies yielded nearly identical results (Supporting Information Fig. S4).) We calculated S^2 as an average
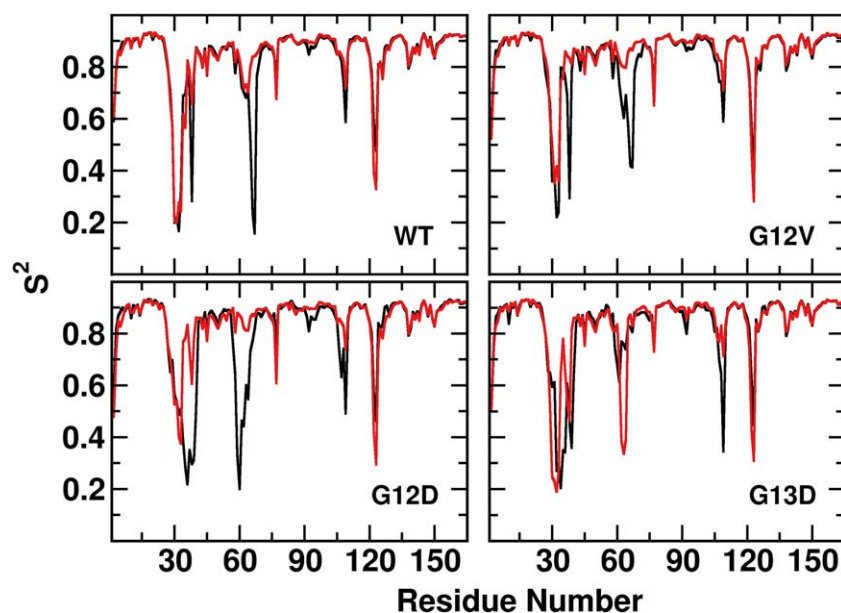
Figure 8

Order parameter of backbone amide bonds. Residue S^2 calculated over the entire trajectory at a sampling frequency of 0.2 ns for H-Ras (black) and K-Ras (red). Qualitatively similar results were obtained at other time windows and sampling frequencies (Supporting Information Figs. S3 and S4). [Color figure can be viewed at wileyonlinelibrary.com]
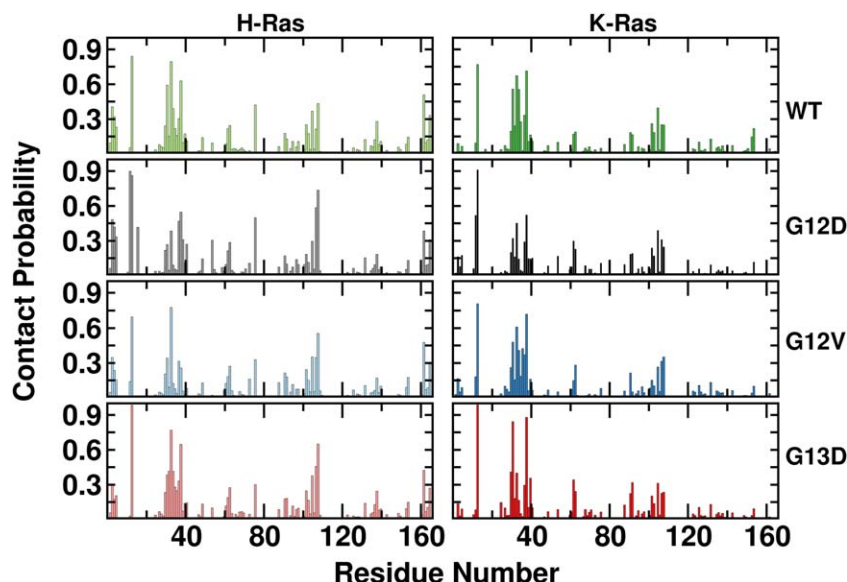
Figure 9

Protein–sodium interaction. Probabilities of sodium ion binding per residue, with binding defined to exist if any heavy atom of a residue was within 4.5 Å of any sodium ion. [Color figure can be viewed at wileyonlinelibrary.com]

over four different time blocks representing 25, 50, 100, and 200 ns time windows (Supporting Information Fig. S3), and without block averaging representing the entire 1 μs time window (Fig. 8). Irrespective of the time window or the simulated system, we obtained S^2 between 0.85 and 0.9 for residues at the core of the protein, consistent with a well-ordered structure. However, significantly lower S^2 (0.5–0.7) were recorded for T2 and G77, and even lower values with large variations for SI, SII, and some other loop regions. Comparison of the different time windows in Supporting Information Figure S4, or the overall data in Supporting Information Figure S4 with that of Figure 8, indicate that for these and other flexible regions the magnitude of the fluctuations somewhat varies with the time window selected, reflecting the existence of fluctuations at multiple timescales. However, all show qualitatively the same behavior. S^2 of SI residues indicate large amplitude motions at almost all timescales, with residues 29–36 displaying the most dynamic behavior in the majority of the mutants. G13D mutants differ from the rest in their lower Y32 order parameter despite damped fluctuations elsewhere. S^2 of residues 20–36 in G12D and G12V H-Ras are significantly different from their K-Ras counterparts, in agreement with our previous conclusion that these mutants sample the more dynamic state 1. Finally, despite some variations among the different timescales that we have analyzed, H-Ras proteins have smaller S^2 at the loop C-terminal to helix 3 whereas K-Ras proteins are more flexible at the loop N-terminal to helix 4 (Supporting Information Fig. S4).

Another notable observation is that S^2 of E37 and D38 are smaller in the H-Ras mutants, suggesting a less ordered effector-binding loop and consistent with the altered SI/SII coupling captured by our difference contact analysis. The S^2 profiles also indicate that SII is significantly more ordered in K-Ras than H-Ras, except for its G12V mutant. K-Ras mutants have smaller S^2 at the β5–α4 loop or L8 (residues 121–123), where there are two amino acid substitutions between H- and K-Ras (AA to PS, see Fig. 1); this is somewhat surprising because we anticipated P121 of K-Ras to decrease rather than increase the dynamics of L8.[87] Conversely, H-Ras proteins harbor smaller S^2 at the α3–β5 loop or L7 (residues 107–110). This appears to be due to the conservative D (H-Ras) to E (K-Ras) substitution at position 107, with E somehow rigidifying L7 and thereby affecting its interaction with solvent (see next section). This may be functionally relevant because conformational changes at α3/L7 have been shown to allosterically modulate Q61's proximity to the nucleotide and thereby affect GTP hydrolysis.[88] Moreover, this loop is part of the allosteric pocket p3,[27,28,30] and therefore the observed differential dynamics may have implications to the development of isoform-selective Ras inhibitors.

Differential solvent interactions

Visual inspection of the trajectories led to an intriguing observation, namely, the active site of the G13D mutants is permanently occupied by a sodium ion. This prompted us to investigate the Na$^+$ binding probabilities in the entire surface of the protein in all simulations (Fig. 9). Binding was defined to exist if any heavy atom of a protein was within 4.5 Å of any Na$^+$ ion of solvent.
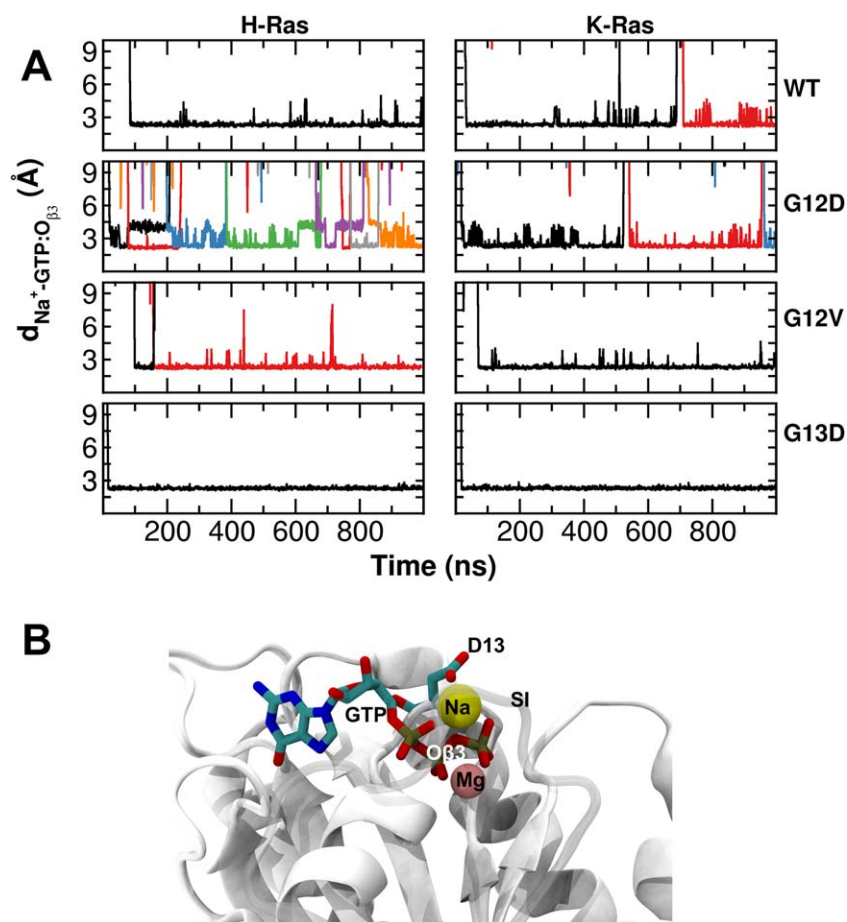
Figure 10

Long-residence sodium-ion binding sites. (**A**) Distance between sodium ion and GTP:Oβ3. Different line colors indicate ion exchange. (**B**) A snapshot of G13D K-Ras showing a sodium ion interacting with GTP. [Color figure can be viewed at wileyonlinelibrary.com]

We found large Na^+ contact probabilities at positions 12 and 13 in the G12D and G13D mutants (Fig. 9), perhaps due to the negative charge of these residues. However, we were surprised to find similarly persistent interactions of Na^+ with many other residues in SI. This is true for all systems, including WT. A closer look at the residues with >20% interaction probability revealed an Na^+ that is tightly bound by GTP:Oβ3 and a number of P-loop residues (Fig. 10). Figure 10 further shows that Na^+ enters the site within a few nanoseconds of the production phase in G12D and G13D, and after some delay in the rest of the proteins. In G13D, once Na^+ has entered, its interaction was so tight that there was no exchange with bulk. In the rest of the proteins there were 1–7 exchange events or significant distance fluctuations, suggesting that binding was somewhat weaker and variable. We speculate that binding of a metal ion at this site induces displacement of Y32 away from the GTP. If so, the interaction of Y32 with the γ-phosphate of GTP commonly observed in GTP analog-bound Ras X-Ray structures, including 4DSO that was used as the starting

structure of our K-Ras simulations, might not be as common in solution at physiologic ionic strength. This interpretation is supported by the lack of Y32–GTP interaction in some of the H-Ras experimental structures (e.g., 1QRA and 2Q21). However, more work is required to draw a definitive conclusion, including potential force field artifacts even though those may not lead to differential effects.

Figure 9 also reveals two other Na^+ binding sites, particularly in the H-Ras proteins. The first involves side chains of E3 and E76 and backbone carbonyl oxygen of Y4, providing for an ion-mediated interaction between E3 and E76 and hence a long-range communication between the N-terminus and SII. The second Na^+ binding site involves side chains of D/E107 and D108 and the backbone carbonyl oxygen of G138. Sodium–protein interaction at this site is more pronounced in H-Ras, and the site has been previously shown to bind divalent ions and allosterically couple L7 to the nucleotide binding site.[88,89] Our results indicate that the site is capable of binding a monovalent ion as well. In addition, L7 is

close to residues 161–164 and therefore metal ion binding at this site can modulate the interaction between D47/E49 and R161/R164. This can affect the allosteric interlobe communication through L3 (residues 46–49) and α5 that has been discussed previously.[41,60,71]

Finally, protein-bound water molecules have long been recognized as intimately linked to structural stability.[90] In a previous study, we characterized three long-residence water molecules (denoted W_1, W_3, and W_4) that primarily interact with K16:O, A83:O, and D126:O, respectively, as well as others (W_2, W_5, and W_6) that are found in the majority of Ras X-ray structures.[91] All of these water molecules are detectable in our simulations, albeit with somewhat variable persistency (Supporting Information Fig. S5). Notably, the deeply buried W_4 coupling the P-loop with α3 rarely exchanges with bulk in all simulations (occupancy >90%). W_1, which is coordinated by A18, H27, and V29, appeared in all simulations with 10–30% occupancy, except in WT and G13D K-Ras. W_2 has a 20–65% occupancy and bridges the backbone of K16 and the side-chain of D57 in G12D/G12V K-Ras and G13D/WT H-Ras; W_3 only exists in G12D H-Ras with an occupancy of 50% while W_6 only occurs in G12V K-Ras and G12D H-Ras with a 40–50% occupancy. Overall, irrespective of isoform or mutation, these structural waters exhibit substantially longer residence times than the most common ps range.[92] This conclusion recapitulates previous observations based on an analysis of all available Ras crystal structures and MD trajectories.[91,93]

CONCLUSION

Ras proteins have been studied extensively not only due to their crucial role in diverse biological processes and cancer but also because they are excellent model systems to study protein structure and dynamics. However, if and how the few amino acid differences at the catalytic domain of different isoforms affect function and how different mutations at the same position give rise to different signal outputs remained undetermined. A major goal of this work was therefore to identify the structural and dynamic basis for the functional diversity of WT H-Ras and K-Ras and their oncogenic mutants G12D, G12V, and G13D. To quantitatively compare conformational fluctuations and interaction patterns among these proteins, we conducted a 1 μs unbiased MD simulation on each system and performed detailed analyses of intraprotein, protein–GTP, and protein–solvent interactions. We analyzed conformational fluctuations using diverse measures of dynamic correlations, relaxation times, NMR order parameter, and other techniques. The results show that the proteins we have studied harbor both shared and unique intraprotein and intermolecular interaction patterns and fluctuations. Differential dynamics and interaction patterns are particularly common in the vicinity of the GTP, but there are also variations at a number of loops distal from the active site. Key results include the following. (i) The switch regions of H-Ras proteins in general and G12V and G12D H-Ras in particular are significantly more flexible than their K-Ras counterparts. In fact, G12D and G12V H-Ras sample conformations that are distinct from the rest of the proteins, including an open switch configuration characteristic of the inactive state 1 of GTP Ras; this state has recently been characterized as a "stable pool of Ras.GTP in the GDP/GTP cycle."[84] In the rest of the simulations, the switches remain closed and similar to the available experimental structures of GTP or GTP-analogue-bound Ras. (ii) There are significant variations in intraprotein interaction networks around the active site, including enhanced coupling between the switches in most of the mutants. This was a result of an interaction between Y71 of SII and E37/D38 of the effector-binding loop. Such differences will likely affect GTP hydrolysis and/or GDP release. (iii) The simulations also revealed a previously underappreciated interaction of metal ions from solvent with the phosphate of GTP and neighboring residues. This interaction is particularly prominent in the G13D mutant of both H-Ras and K-Ras. In these mutants, entrance of a sodium ion is directly coupled with a rotation of the D13 side-chain toward the phosphate moiety, where it participates in coordinating the metal ion. Ion binding also appears to be contributing to the displacement of Y32 from its position capping the GTP, and Y32 is significantly disordered in G13D mutants. This suggests a direct potential effect on nucleotide exchange that is associated with Y32 movement. (iv) We observed differences in protein–solvent interaction and fluctuations distal from the active site, including at loops L7 and L8. For example, K-Ras mutants are more dynamic at L8 than their H-Ras counterparts, indicating that effects of isoform variation and P-loop mutation are not limited to local side-chain reorganizations at the active site. The observed differences in interaction with water and ions are significant in light of previous observations by us[91] and Mattos and colleagues[93] on the role of water networks on Ras allostery. (v) The differential fluctuations and interaction patterns listed above and many others described in this article have implications for functional specialization including in GTPase activity and effector interaction. For example, oncogenicity of mutants that favor the state 1 conformation such as G13D H-Ras is likely caused by a different mechanism than those that favor state 2. We caution, however, that transition between these two states is slow and might require longer than 1 μs simulation. Quantifying the population of these states in each isoform and mutant via longer simulations or using enhanced sampling methods would be a worthy future endeavor.

Discovery Environment (XSEDE Project: MCB150054) for computational resources.

REFERENCES

1. Cox AD, Der CJ. Ras history: the saga continues. Small GTPases 2010;1:2–27.
2. Barbacid M. Ras genes. Annu Rev Biochem 1987;56:779–827.
3. Bourne HR, Sanders DA, McCormick F. The GTPase superfamily: a conserved switch for diverse cell functions. Nature 1990;348:125–132.
4. Hall BE, Bar-Sagi D, Nassar N. The structural basis for the transition from Ras-GTP to Ras-GDP. Proc Natl Acad Sci USA 2002;99:12138–12142.
5. Shields JM, Pruitt K, McFall A, Shaub A, Der CJ. Understanding Ras:'it ain't over'til it's over'. Trends Cell Biol 2000;10:147–154.
6. Vetter IR, Wittinghofer A. The guanine nucleotide-binding switch in three dimensions. Science 2001;294:1299–1304.
7. Avruch J, Zhang X-f, Kyriakis JM. Raf meets Ras: completing the framework of a signal transduction pathway. Trends Biochem Sci 1994;19:279–283.
8. Wittinghofer A, Nassar N. How Ras-related proteins talk to their effectors. Trends Biochem Sci 1996;21:488–491.
9. Nan X, Tamgüney TM, Collisson EA, Lin LJ, Pitt C, Galeas J, Lewis S, Gray JW, McCormick F, Chu S. Ras-GTP dimers activate the mitogen-activated protein kinase (MAPK) pathway. Proc Natl Acad Sci USA 2015;112:7996–8001.
10. Zhou Y, Hancock JF. Ras nanoclusters: versatile lipid-based signaling platforms. Biochim Biophys Acta, Mol Cell Res 2015;1853:841–849.
11. Abankwa D, Gorfe AA, Inder K, Hancock JF. Ras membrane orientation and nanodomain localization generate isoform diversity. Proc Natl Acad Sci USA 2010;107:1130–1135.
12. Mazhab-Jafari MT, Marshall CB, Smith MJ, Gasmi-Seabrook GM, Stathopulos PB, Inagaki F, Kay LE, Neel BG, Ikura M. Oncogenic and RASopathy-associated K-RAS mutations relieve membrane-dependent occlusion of the effector-binding site. Proc Natl Acad Sci USA 2015;112:6625–6630.
13. Prakash P, Gorfe AA. Membrane orientation dynamics of lipid-modified small GTPases. Small GTPases 2016;1–10.
14. Gorfe AA, Hanzal-Bayer M, Abankwa D, Hancock JF, McCammon JA. Structure and dynamics of the full-length lipid-modified H-Ras protein in a 1,2-dimyristoylglycero-3-phosphocholine bilayer. J Med Chem 2007;50:674–684.
15. Yan J, Roy S, Apolloni A, Lane A, Hancock JF. Ras isoforms vary in their ability to activate Raf-1 and phosphoinositide 3-kinase. J Biol Chem 1998;273:24052–24056.
16. Castellano E, Santos E. Functional specificity of ras isoforms so similar but so different. Genes Cancer 2011;2:216–231.
17. Abankwa D, Gorfe AA, Hancock JF. Ras nanoclusters: molecular structure and assembly. Semin Cell Dev Biol 2007;18:599–607.
18. Namba H, Rubin SA, Fagin JA. Point mutations of ras oncogenes are an early event in thyroid tumorigenesis. Mol Endocrinol 1990;4:1474–1479.
19. Visvanathan K, Pocock R, Summerhayes I. Preferential and novel activation of H-ras in human bladder carcinomas. Oncogene Res 1987;3:77–86.
20. Bos JL, Fearon ER, Hamilton SR, Verlaan-de Vries M, van Boom JH, van der Eb AJ, Vogelstein B. Prevalence of ras gene mutations in human colorectal cancers. Nature 1987;327:293–297.
21. Almoguera C, Shibata D, Forrester K, Martin J, Arnheim N, Perucho M. Most human carcinomas of the exocrine pancreas contain mutant cK-ras genes. Cell 1988;53:549–554.
22. Prior IA, Lewis PD, Mattos C. A Comprehensive Survey of Ras Mutations in Cancer. Cancer Res 2012;72:2457–2467.
23. van 't Veer LJ, Burgering BM, Versteeg R, Boot AJ, Ruiter DJ, Osanto S, Schrier PI, Bos JL. N-ras mutations in human cutaneous melanoma from sun-exposed body sites. Mol Cell Biol 1989;9:3114–3116.
24. Bos JL. Ras oncogenes in human cancer: a review. Cancer Res 1989;49:4682–4689.
25. Riely GJ, Marks J, Pao W. KRAS mutations in non-small cell lung cancer. Proc Am Thorac Soc 2009;6:201–205.
26. Ostrem JM, Shokat KM. Direct small-molecule inhibitors of KRAS: from structural insights to mechanism-based design. Nat Rev Drug Discovery 2016;15:771–785.
27. Prakash P, Hancock JF, Gorfe AA. Binding hotspots on K-ras: consensus ligand binding sites and other reactive regions from probe-based molecular dynamics analysis. Proteins Struct Funct Bioinf 2015;83:898–909.
28. Prakash P, Sayyed-Ahmad A, Gorfe AA. pMD-membrane: a method for ligand binding site identification in membrane-bound proteins. PLoS Comput Biol 2015;11:e1004469.
29. Hocker HJ, Cho KJ, Chen CY, Rambahal N, Sagineedu SR, Shaari K, Stanslas J, Hancock JF, Gorfe AA. Andrographolide derivatives inhibit guanine nucleotide exchange and abrogate oncogenic Ras function. Proc Natl Acad Sci USA 2013;110:10201–10206.
30. Grant BJ, Lukman S, Hocker HJ, Sayyah J, Brown JH, McCammon JA, Gorfe AA. Novel allosteric sites on Ras for lead generation. PLoS One 2011;6:e25711.
31. Cox AD, Fesik SW, Kimmelman AC, Luo J, Der CJ. Drugging the undruggable RAS: mission possible?. Nat Rev Drug Discov 2014;13:828–851.
32. Baines AT, Xu D, Der CJ. Inhibition of Ras for cancer treatment: the search continues. Future Med Chem 2011;3:1787–1808.
33. Hancock JF, Magee AI, Childs JE, Marshall CJ. All ras proteins are polyisoprenylated but only some are palmitoylated. Cell 1989;57:1167–1177.
34. Hancock JF. Ras proteins: different signals from different locations. Nat Rev Mol Cell Biol 2003;4:373–385.
35. Vojtek AB, Der CJ. Increasing complexity of the Ras signaling pathway. J Biol Chem 1998;273:19925–19928.
36. Boguski MS, McCormick F. Proteins regulating Ras and its relatives. Nature 1993;366:643–654.).
37. Stolze B, Reinhart S, Bulllinger L, Fröhling S, Scholl C. Comparative analysis of KRAS codon 12, 13, 18, 61, and 117 mutations using human MCF10A isogenic cell lines. Sci Rep 2015;5.
38. Spoerner M, Hozsa C, Poetzl JA, Reiss K, Ganser P, Geyer M, Kalbitzer HR. Conformational states of human rat sarcoma (Ras) protein complexed with its natural ligand GTP and their role for effector interaction and GTP hydrolysis. J Biol Chem 2010;285:39768–39778.
39. Lu S, Jang H, Muratcioglu S, Gursoy A, Keskin O, Nussinov R, Zhang J. Ras conformational ensembles, allostery, and signaling. Chem Rev 2016;116:6607–6665.
40. Marcus K, Mattos C. Direct attack on RAS: intramolecular communication and mutation-specific effects. Clin Cancer Res 2015;21:1810–1818.
41. Grant BJ, Gorfe AA, McCammon JA. Ras conformational switching: simulating nucleotide-dependent conformational transitions with accelerated molecular dynamics. PLoS Comput Biol 2009;5:e1000325.
42. Futatsugi N, Tsuda M. Molecular dynamics simulations of Gly-12→Val mutant of p21 ras: dynamic inhibition mechanism. Biophys J 2001;81:3483–3488.
43. Lukman S, Grant BJ, Gorfe AA, Grant GH, McCammon JA. The distinct conformational dynamics of K-Ras and H-Ras A59G. PLoS Comput Biol 2010;6:e1000922.
44. Shurki A, Warshel A. Why does the Ras switch "break" by oncogenic mutations?. Proteins Struct Funct Bioinf 2004;55:1–10.
45. Khrenova MG, Grigorenko BL, Mironov VA, Nemukhin AV. Why does mutation of Gln61 in Ras by the nitro analog NGln maintain activity of Ras-GAP in hydrolysis of guanosine triphosphate?. Proteins 2015;83:2091–2099.

46. Khrenova MG, Mironov VA, Grigorenko BL, Nemukhin AV. Modeling the role of G12V and G13V Ras mutations in the Ras-GAP-catalyzed hydrolysis reaction of guanosine triphosphate. Biochemistry 2014;53:7093–7099.

47. Mironov VA, Khrenova MG, Lychko LA, Nemukhin AV. Computational characterization of the chemical step in the GTP hydrolysis by Ras-GAP for the wild-type and G13V mutated Ras. Proteins 2015;83:1046–1053.

48. Abankwa D, Gorfe AA, Hancock JF. Ras nanoclusters: molecular structure and assembly. Semin Cell Dev Biol 2007;18:599–607.

49. Prakash P, Zhou Y, Liang H, Hancock JF, Gorfe AA. Oncogenic K-Ras binds to an anionic membrane in two distinct orientations: a molecular dynamics analysis. Biophys J 2016;110:1125–1138.

50. Li Z, Cao S, Buck M. K-Ras at anionic membranes: orientation, orientation…orientation. Recent simulations and experiments. Biophys J 2016;110:1033–1035.

51. Baussand J, Kleinjung J. Specific conformational states of Ras GTPase upon effector binding. J Chem Theory Comput 2012;9:738–749.

52. Harding A, Hancock JF. Ras nanoclusters: combining digital and analog signaling. Cell Cycle 2008;7:127–134.

53. Geyer M, Schweins T, Herrmann C, Prisner T, Wittinghofer A, Kalbitzer HR. Conformational transitions in p21 ras and in its complexes with the effector protein Raf-RBD and the GTPase activating protein GAP. Biochemistry 1996;35:10308–10320.

54. Herrmann C. Ras–effector interactions: after one decade. Curr Opin Struct Biol 2003;13:122–129.

55. Pacold ME, Suire S, Perisic O, Lara-Gonzalez S, Davis CT, Walker EH, Hawkins PT, Stephens L, Eccleston JF, Williams RL. Crystal structure and functional analysis of Ras binding to its effector phosphoinositide 3-kinase γ. Cell 2000;103:931–944.

56. Ford B, Hornak V, Kleinman H, Nassar N. Structure of a transient intermediate for GTP hydrolysis by ras. Structure 2006;14:427–436.

57. Hunter JC, Manandhar A, Carrasco MA, Gurbani D, Gondi S, Westover KD. Biochemical and structural analysis of common cancer-associated KRAS mutations. Mol Cancer Res 2015;13:1325–1335.

58. John J, Frech M, Wittinghofer A. Biochemical properties of Ha-ras encoded p21 mutants and mechanism of the autophosphorylation reaction. J Biol Chem 1988;263:11792–11799.

59. Herrmann C, Martin GA, Wittinghofer A. Quantitative analysis of the complex between p21 and the ras-binding domain of the human raf-1 protein kinase. J Biol Chem 1995;270:2901–2905.

60. Gorfe AA, Grant BJ, McCammon JA. Mapping the nucleotide and isoform-dependent structural and dynamical features of Ras proteins. Structure 2008;16:885–896.

61. Ryckaert JPCG, Berendsen HJC. Numerical integration of the Cartesian equations of motion of a system with constraints: molecular dynamics of n-Alkanes. J Comput Phys 1977;23

62. Darden T, York D, Pedersen L. Particle mesh Ewald: an N·log (N) method for Ewald sums in large systems. J Chem Phys 1993;98:10089–10092.

63. Phillips JC, Braun R, Wang W, Gumbart J, Tajkhorshid E, Villa E, Chipot C, Skeel RD, Kale L, Schulten K. Scalable molecular dynamics with NAMD. J Comput Chem 2005;26:1781–1802.

64. Buck M, Bouguet-Bonnet S, Pastor RW, MacKerell AD. Jr. Importance of the CMAP correction to the CHARMM22 protein force field: dynamics of hen lysozyme. Biophys J 2006;90:L36–L38.

65. Johnson QR, Lindsay RJ, Nellas RB, Fernandez EJ, Shen T. Mapping allostery through computational glycine scanning and correlation analysis of residue–residue contacts. Biochemistry 2015;54:1534–1541.

66. Doshi U, Holliday MJ, Eisenmesser EZ, Hamelberg D. Dynamical network of residue–residue contacts reveals coupled allosteric effects in recognition, catalysis, and mutation. Proc Natl Acad Sci USA 2016;113:4735–4740.

67. Nussinov R, Tsai C-J. Allostery without a conformational change? Revisiting the paradigm. Curr Opin Struct Biol 2015;30:17–24.

68. Ma J, Karplus M. Molecular switch in signal transduction: reaction paths of the conformational changes in ras p21. Proc Natl Acad Sci USA 1997;94:11905–11910.

69. Ma J, Karplus M. Ligand-induced conformational changes in ras p21: a normal mode and energy minimization analysis. J Mol Biol 1997;274:114–131.

70. Kobayashi C, Saito S. Relation between the conformational heterogeneity and reaction cycle of Ras: molecular simulation of Ras. Biophys J 2010;99:3726–3734.

71. Prakash P, Gorfe AA. Lessons from computer simulations of Ras proteins in solution and in membrane. Biochim Biophys Acta, Gen Subj 2013;1830:5211–5218.

72. Villa A, Stock G. What NMR relaxation can tell us about the internal motion of an RNA hairpin: a molecular dynamics simulation study. J Chem Theory Comput 2006;2:1228–1236.

73. Gu Y, Li D-W, Brüschweiler R. NMR order parameter determination from long molecular dynamics trajectories for objective comparison with experiment. J Chem Theory Comput 2014;10:2599–2607.

74. Scheffzek K, Ahmadian MR, Kabsch W, Wiesmüller L, Lautwein A, Schmitz F, Wittinghofer A. The Ras–RasGAP complex: structural basis for GTPase activation and its loss in oncogenic Ras mutants. Science 1997;277:333–339.

75. Hall BE, Yang SS, Boriack-Sjodin PA, Kuriyan J, Bar-Sagi D. Structure-based mutagenesis reveals distinct functions for Ras switch 1 and switch 2 in Sos-catalyzed guanine nucleotide exchange. J Biol Chem 2001;276:27629–27637.

76. Knihtila R, Holzapfel G, Mattos C. Study of Ras catalytic mechanism of intrinsic hydrolysis of GTP. FASEB J 2013;27:831.10–831.10.

77. Sayyed-Ahmad A, Cho K-J, Hancock JF, Gorfe AA. Computational equilibrium thermodynamic and kinetic analysis of K-Ras dimerization through an effector binding surface suggests limited functional role. J Phys Chem B 2016;120:8547–8556.

78. Sun Q, Burke JP, Phan J, Burns MC, Olejniczak ET, Waterson AG, Lee T, Rossanese OW, Fesik SW. Discovery of small molecules that bind to K-Ras and inhibit Sos-mediated activation. Angew Chem 2012;124:6244–6247.

79. Maurer T, Garrenton LS, Oh A, Pitts K, Anderson DJ, Skelton NJ, Fauber BP, Pan B, Malek S, Stokoe D, Ludlam MJ. Small-molecule ligands bind to a distinct pocket in Ras and inhibit SOS-mediated nucleotide exchange activity. Proc Natl Acad Sci USA 2012;109:5299–5304.

80. Buhrman G, Casey O, Zerbe B, Kearney BM, Napoleon R, Kovrigina EA, Vajda S, Kozakov D, Kovrigin EL, Mattos C. Analysis of binding site hot spots on the surface of Ras GTPase. J Mol Biol 2011;413:773–789.

81. Prakash P, Sayyed-Ahmad A, Cho KJ, Dolino DM, Chen W, Li H, Grant BJ, Hancock JF, Gorfe AA. Computational and biochemical characterization of two partially overlapping interfaces and multiple weak-affinity K-Ras dimers. Sci Rep 2017;7:40109.

82. Spoerner M, Herrmann C, Vetter IR, Kalbitzer HR, Wittinghofer A. Dynamic properties of the Ras switch I region and its importance for binding to effectors. Proc Natl Acad Sci USA 2001;98:4944–4949.

83. Spoerner M, Nuehs A, Ganser P, Herrmann C, Wittinghofer A, Kalbitzer HR. Conformational states of Ras complexed with the GTP analogue GppNHp or GppCH2p: implications for the interaction with effector proteins. Biochemistry 2005;44:2225–2236.

84. Matsumoto S, Miyano N, Baba S, Liao J, Kawamura T, Tsuda C, Takeda A, Yamamoto M, Kumasaka T, Kataoka T, Shima F. Molecular mechanism for conformational dynamics of Ras.GTP elucidated from in-situ structural transition in crystal. Sci Rep 2016;6:25931.

85. Tong L, de Vos AM, Milburn MV, Kim S-H. Crystal structures at 2.2 Å resolution of the catalytic domains of normal ras protein and

an oncogenic mutant complexed with GDP. J Mol Biol 1991;217: 503–516.

86. Araki M, Shima F, Yoshikawa Y, Muraoka S, Ijiri Y, Nagahara Y, Shirono T, Kataoka T, Tamura A. Solution structure of the state 1 conformer of GTP-bound H-Ras protein and distinct dynamic properties between the state 1 and state 2 conformers. J Biol Chem 2011;286:39644–39653.

87. Krieger F, Möglich A, Kiefhaber T. Effect of proline and glycine residues on dynamics and barriers of loop formation in polypeptide chains. J Am Chem Soc 2005;127:3346–3352.

88. Buhrman G, Holzapfel G, Fetics S, Mattos C. Allosteric modulation of Ras positions Q61 for a direct role in catalysis. Proc Natl Acad Sci USA 2010;107:4931–4936.

89. O'Connor C, Kovrigin EL. Characterization of the second ion-binding site in the G domain of H-Ras. Biochemistry 2012;51:9638–9646.

90. Mattos C. Protein–water interactions in a dynamic world. Trends Biochem Sci 2002;27:203–208.

91. Prakash P, Sayyed-Ahmad A, Gorfe AA. The role of conserved waters in conformational transitions of Q61H K-ras. PLoS Comput Biol 2012;8:e1002394.

92. Denisov VP, Halle B. Protein hydration dynamics in aqueous solution. Faraday Discuss 1996;103:227–244.

93. Kearney BM, Johnson CW, Roberts DM, Swartz P, Mattos C. DRoP: a water analysis program identifies Ras-GTP-specific pathway of communication between membrane-interacting regions and the active site. J Mol Biol 2014;426:611–629.